MICROSTRUCTURAL MECHANISMS OF CREEP IN GAMMA Ti-52Al

ALENA ORLOVÁ, KVĚTA KUCHAŘOVÁ, ANTONÍN DLOUHÝ*

Institute of Physics of Materials, Academy of Sciences of the Czech Republic, Žižkova 22, 616 62 Brno, Czech Republic

The present work investigates three typical dislocation and twinning structures resulting from creep in the Ti-52Al intermetallic – irregular 3D dislocation network (type I), regular subgrains and their boundaries (type II) and the system of deformation twins (type III). The microstructures observed by transmission electron microscopy are analyzed and the emphasis is given to deformation modes and possible reactions of various types of dislocations that can govern creep in the intermetallic compound.

1. Introduction

Dislocation configurations formed in polycrystalline materials during creep are influenced by grain size, misorientation of neighbouring grains and by more complicated conditions of dislocation glide – the activity of several glide systems [1]. A recent investigation of the microstructural development in the course of the high temperature creep in the gamma Ti-52Al intermetallic phase [2] revealed three microstructural types, co-existing and developing in parallel in neighbouring grains of the tetragonal $L1_0$ compound. The irregular 3D dislocation network (type I), regular subgrains and their boundaries (type II) and the system of deformation twins (type III) were identified by transmission electron microscopy (TEM). The material states after creep were also observed by the conventional light microscopy. The microstructures always form due to the activity of three fundamental deformation modes that contribute to the overall creep strain [3]: (i) the glide motion of ordinary dislocations, (ii) the glide of superdislocations and (iii) the nucleation and growth of deformation twins. In the present paper the emphasis is given to typical local configurations in order to assess deformation mechanisms that govern the microstructural development and control creep rate.

---

*corresponding author, e-mail: dlouhy@ipm.cz

2. Material and experimental techniques

The single phase gamma Ti-52at.%Al was supplied by IRC Birmingham, UK. The melting, casting, and HIP treatment (details described in the previous paper [2]) resulted in a highly irregular microstructure of large grains with numerous annealing twins. Smaller round grains growing from the internal interfaces indicated some recrystallization during HIP. Creep tests in compression were performed in purified argon atmosphere on cylindrical specimens 5 mm in diameter and 12 mm in height under a constant applied stress of 250 MPa and at temperature of 1100 K. The development of microstructures was investigated after creep exposures interrupted at different creep strains. The complete list of investigated specimens, their creep exposures and the corresponding microstructural data is presented in Table 1 of the previous study [2]. Table 1 of the present paper summarizes only data relevant to the specimens investigated in this study. Some of the typical microstructures documented in the foregoing TEM investigation [2] were chosen for a detailed analysis in the present work.

After the creep exposures the cylindrical specimens were cut axially into two halves. The surface of one half was polished and investigated by the conventional light microscopy. The double refracting layer and polarized light improved the resolution of microstructural features. The other half was cut by spark erosion into platelets suitable for a preparation of thin TEM foils. The TEM foils were further thinned by a standard procedure, i.e. by grinding on emery papers and double jet electropolishing in TENUPOL. TEM observations were mostly performed in the bright-field imaging mode where two-beam conditions with selected diffraction vectors g provided sufficient image contrast. The two-beam conditions with gs chosen from the types {111}, {200} or {220} give a full contrast of the ordinary dislocations with $1/2\langle110\rangle$-type of Burgers vector. These dislocations (type $\langle a\rangle$)

T a b l e 1. Specimens investigated in the present study, parameters of their creep exposure at 1100 K and 250 MPa and related quantitative microstructural data

Specimen	Total creep exposure time [s]	Total strain ε	Dislocation density $[10^{13} \text{ m}^{-2}]$		Twin parameters [nm]		Remark
			ρ_{total}	$\rho_{\langle c\rangle}$	Spacing λ	Width w	
TA28	601	0.065	1.42 ± 0.20	0.44 ± 0.05	484 ± 59	83 ± 4	
TA18	1682	0.08	8.07 ± 0.77	3.94 ± 0.22	$664 \pm 37^{*}$ $\approx 8500^{**}$	178 ± 8	TEM*) LIGHT**)
TA9	4208	0.36	6.71 ± 0.76	2.43 ± 0.64	380 ± 60	75 ± 29	

ρ_{total} – overall dislocation density, $\rho_{\langle c\rangle}$ – density of $\langle c\rangle$ dislocations (see text), λ – mean twin spacing, w – mean twin width.
Twin spacing data obtained by TEM *) and the light microscopy **).

are not visible or exhibit only a residual contrast under the imaging condition with $g = (002)$ which is, however, favourable for the full contrast of dislocations with a non-zero $\langle c \rangle$ component of the Burgers vector ($\langle c \rangle$ dislocations).

The observation of the same foil area under different diffraction conditions, one of them being $g = (002)$, can thus separate the $\langle a \rangle$ and $\langle c \rangle$ dislocations. This technique, applied in [2] to quantitatively assess the dislocation densities $\rho_{\langle a \rangle}$ and $\rho_{\langle c \rangle}$ of the respective dislocations, will also be used in the present study to identify individual dislocations on the basis of $g \cdot b = 0$ criteria (b is the dislocation Burgers vector). We note that the total dislocation density ρ_{total} given in Table 1 represents the sum of $\rho_{\langle a \rangle}$ and $\rho_{\langle c \rangle}$.

3. Analysis of microstructures

3.1 Three-dimensional network of dislocations

Figures 1a and b show a typical arrangement of dislocations in grains in which the 3D dislocation network represents the dominant microstructural type. Dislocations projected into the plane of TEM micrograph invoke an impression that lines tend to be oriented along two directions. The lattice cell projection method [4]
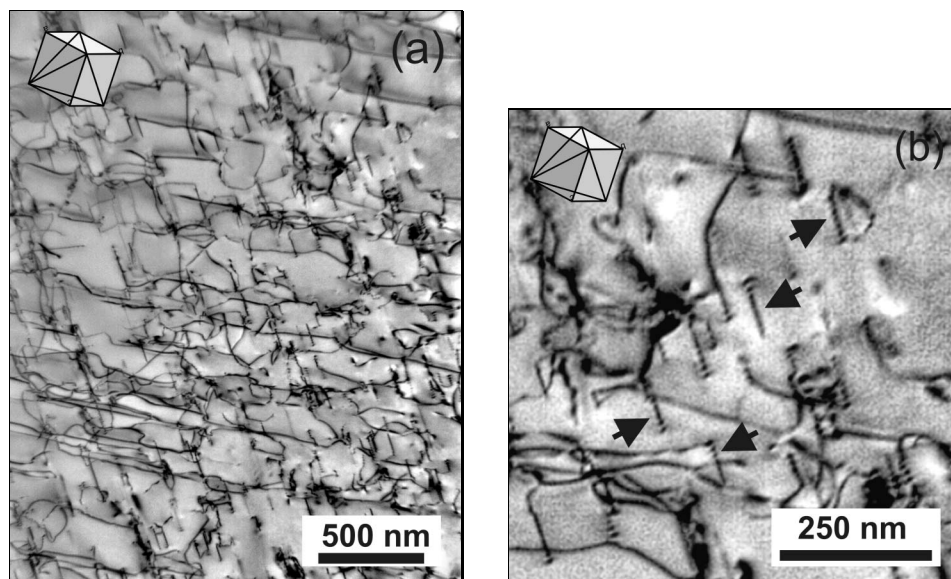
Fig. 1. (a) Three dimensional dislocation network observed after 0.08 strain accumulated at 1100 K and 250 MPa in which dislocation lines tend to be oriented along two crystallographic directions (specimen TA18). (b) Some of the narrow planar faults indicated by arrows exhibit a typical fringed contrast under $g = (1\bar{1}1)$. See text for further details.

indicates that one of these two directions corresponds to the edge-on projection of the $(1\bar{1}1)$ reflection plane. The other characteristic direction in Fig. 1a is almost parallel to the $[1\bar{1}0]$ crystallographic direction.

As the $(1\bar{1}1)$ reflection plane is also the slip plane for [110]-type ordinary dislocations and [011]- and $[10\bar{1}]$-type superdislocations, these line defects, when fully located in their slip plane, should exhibit only a residual TEM contrast aligned with the plane trace. Indeed, there are numerous contrast features like this in Fig. 1a. However, there also are many lines that are in full contrast while they are still aligned with the trace of the $(1\bar{1}1)$ reflection plane, arrows in Fig. 1b highlight some of them. A more detailed analysis suggests that these line defects exhibit a TEM contrast similar to narrow stacking fault ribbons with the width of about 5–10 nm. The analysis also shows that the plane in which fault ribbons extend is not parallel with the $(1\bar{1}1)$ reflection plane. All these experimental findings thus lead to at least two possible scenarios that would rationalize the core structure of corresponding dislocations: (i) either the TEM contrast in question is due to screw (super)dislocations of the [110], [011] or $[10\bar{1}]$-type of Burgers vector the dissociation of which is planar, however, not in the $(1\bar{1}1)$ reflection plane, (ii) or the corresponding dislocations move in the $(1\bar{1}1)$ reflection plane and their core structure is non-planar. All these cases were discussed in the literature, e.g. [3, 5, 6].

Besides the extended core structure, the alignment of dislocations along the $[1\bar{1}0]$ crystallographic direction in Fig. 1 could also be associated with either deep Peierls energy valleys along the $\langle 110 \rangle$ directions which may block the $\langle 110 \rangle$-type screw ordinary dislocations [7] or the pinning effect of tall jogs which were shown to control the motion of $\langle 110 \rangle$-type screw dislocations [8, 9]. All the three mechanisms may contribute to the observed alignment of dislocations in grains where the 3D dislocation network represents the dominant type of microstructure after creep.

3.2 Regular dislocation boundaries

Two examples of dislocation boundaries formed during creep are documented in Figs. 2 and 3. These boundaries were found in grains that exhibited a tendency to subgrain formation. The first example shown in Fig. 2 is a twist subgrain boundary composed of two families of nearly screw $\langle 110 \rangle$-type dislocations. Both dislocation families are in full contrast under $\boldsymbol{g} = (020)$ in Fig. 2a and the boundary exhibits quite regular mesh structure. TEM micrographs in Figs. 2b and c present the same part of the boundary under $\boldsymbol{g} = (2\bar{2}0)$ and $\boldsymbol{g} = (220)$ which, respectively, provide the full contrast for the $[1\bar{1}0]$-type (Fig. 2b) and the [110]-type (Fig. 2c) screw dislocations whereas the other dislocation family is out of contrast in the respective micrographs. While the twist boundary in Fig. 2 is solely composed of the ordinary dislocations, the other boundary in Fig. 3 contains, in addition, also dislocations or dislocation reaction products that are $\langle c \rangle$-component dislocations. This fact stems
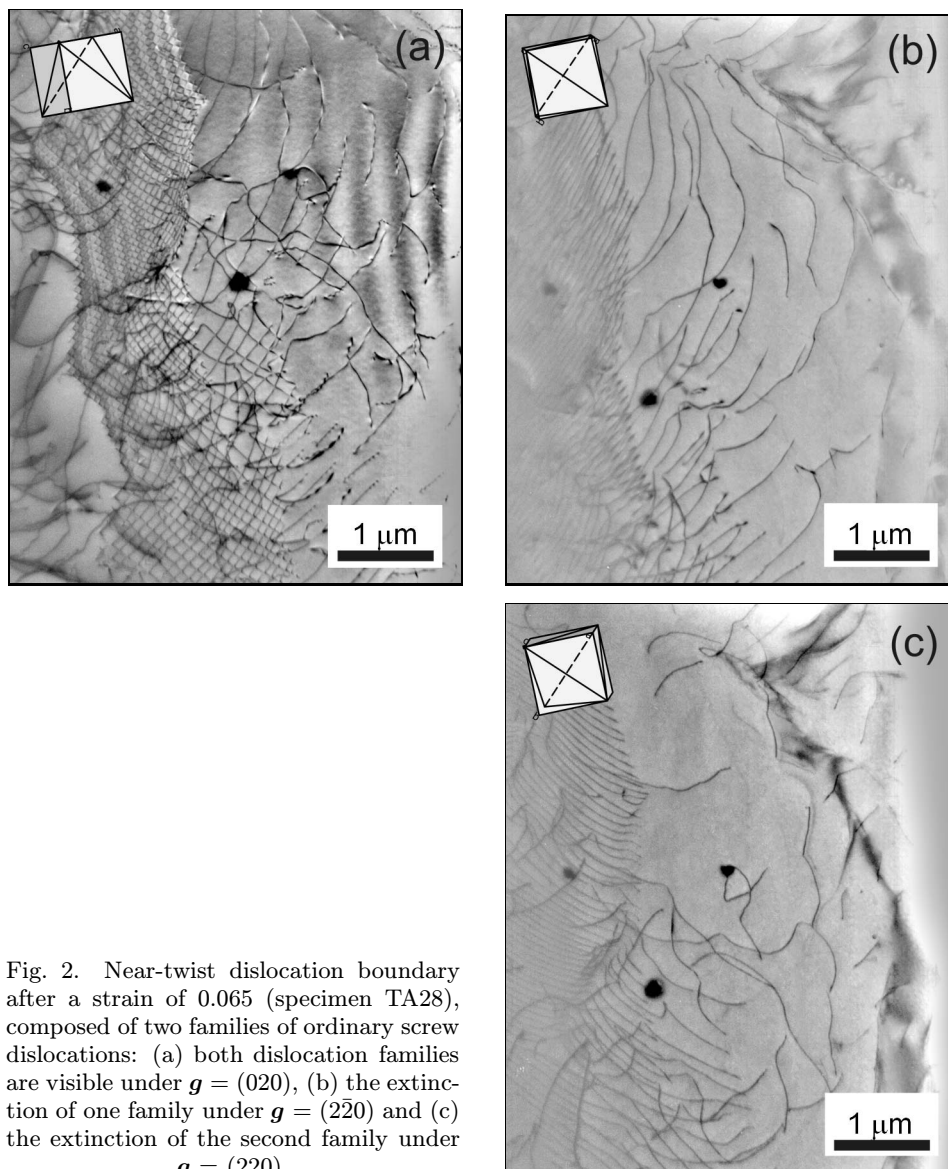
Fig. 2. Near-twist dislocation boundary after a strain of 0.065 (specimen TA28), composed of two families of ordinary screw dislocations: (a) both dislocation families are visible under $g = (020)$, (b) the extinction of one family under $g = (2\bar{2}0)$ and (c) the extinction of the second family under $g = (220)$.

from the TEM contrast analysis where, in Fig. 3a, the selected diffraction vector $g = (1\bar{1}\bar{1})$ provides good image conditions for all dislocations except the ones with [110], [0$\bar{1}$1] and [101]-type of Burgers vector. On the other hand, $g = (002)$ in Fig. 3b gives full contrast only to all dislocations with the non-zero $\langle c \rangle$-component of Burgers vector. A more detailed study of dislocation configurations by means of stereo-pair method [4] suggests that majority of dislocations in the investigated area
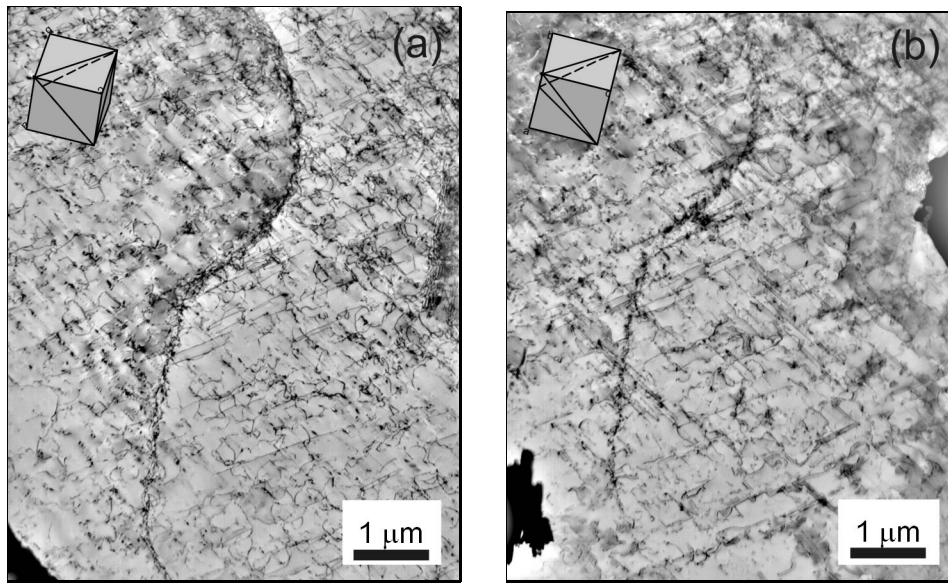
Fig. 3. Dislocation boundary observed after strain of 0.08 (specimen TA18) is composed of both the ordinary and $\langle c \rangle$-component dislocations: (a) $\boldsymbol{g} = (1\bar{1}\bar{1})$, (b) $\boldsymbol{g} = (002)$.

are $\langle c \rangle$-component dislocations aligned with the $[0\bar{1}1]$- and $[011]$-crystallographic directions. There are two possible arrangements: (i) both dislocation families are either the pure screw or $60°$, then a potential exists for energetically neutral and favourable dislocation reactions

$$[0\bar{1}1] + [011] \rightarrow [002] \rightarrow [001] + [001], \tag{1}$$
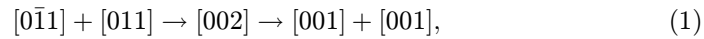
(ii) or one family is screw and the other $60°$ and then an energetically favourable reaction

$$[101] + [0\bar{1}\bar{1}] \rightarrow [1\bar{1}0] \rightarrow 1/2[1\bar{1}0] + 1/2[1\bar{1}0] \tag{2}$$
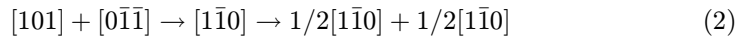
may contribute to the formation of dislocation nodes. Reactions Eqs. (1) and (2) result in sessile dislocation segments that would stabilize the observed dislocation network. A more complete $\boldsymbol{g} \cdot \boldsymbol{b}$ analysis and TEM contrast simulations are required to explore fully the nature and composition of dislocation boundaries similar to the one shown in Fig. 3.

3.3 Twinning and related phenomena

The third microstructural type assessed in the present study was found in the specimen volume in which deformation twinning contributed to the creep strain accumulation. TEM micrographs in Figs. 4 and 5 illustrate this type of microstructure in detail. As it is presented in Table 1, these microstructures were quantitatively described using a mean twin spacing λ and a mean twin width w. The micrograph in Fig. 4a shows a typical arrangement of deformation twins with a corresponding selected area diffraction (SAD) presented in Fig. 4b. The SAD was obtained from
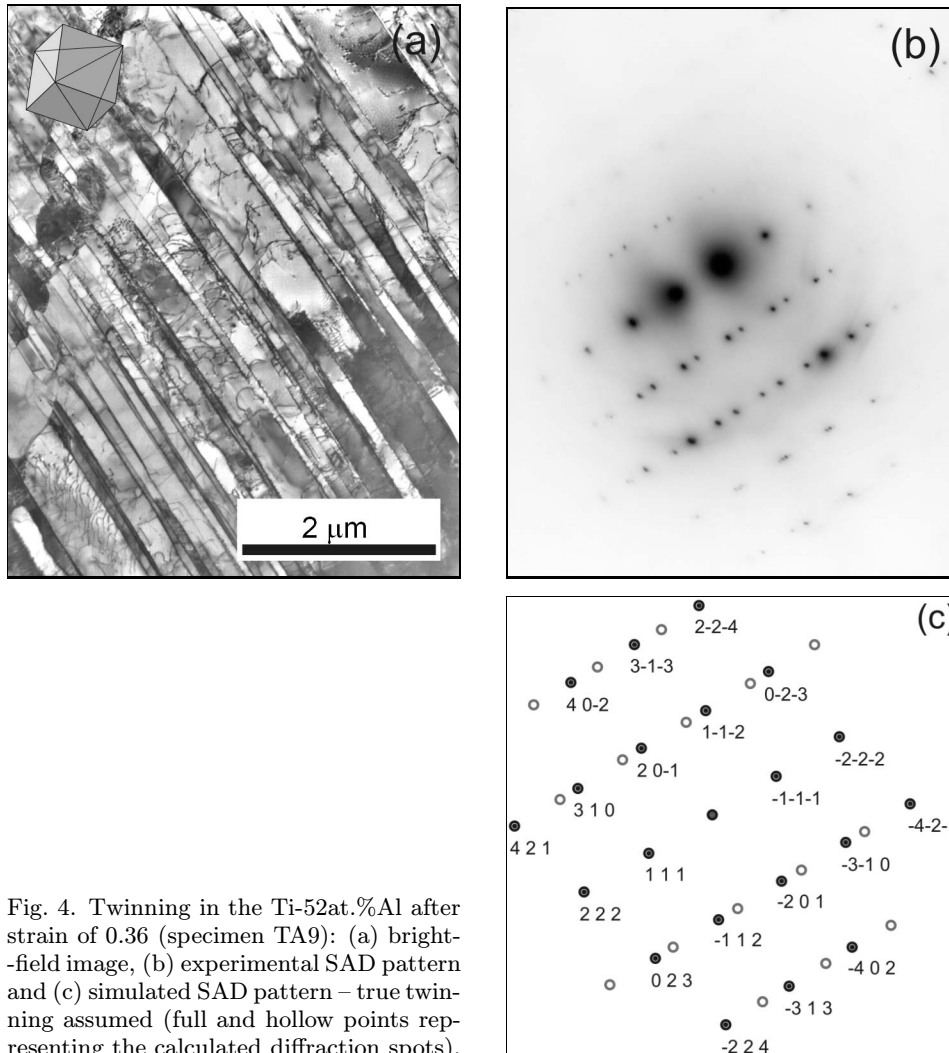
Fig. 4. Twinning in the Ti-52at.%Al after strain of 0.36 (specimen TA9): (a) bright-field image, (b) experimental SAD pattern and (c) simulated SAD pattern – true twinning assumed (full and hollow points representing the calculated diffraction spots).
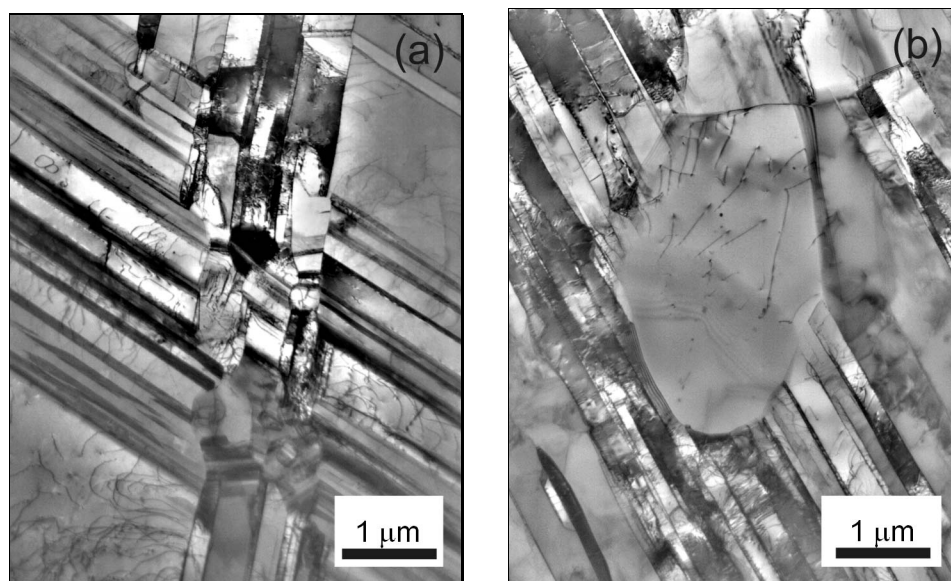
Fig. 5. More complex twinned structures: (a) High strain localization in the cross-twinning area can serve as a driving force to initiate the recrystallization process (strain 0.065, specimen TA28); (b) Further growth of the recrystallized grains was observed after accumulated strain of 0.36 (specimen TA9).

the central part of the area shown in Fig. 4a. The SAD pattern is analyzed in Fig. 4c where a full match between the experimental SAD and a computer-simulated pattern was only obtained under the assumption of a true-twin type relationship. This result supports the interpretation of the structure documented in Fig. 4a as a sequence of true twins (deformation twins) in the gamma phase. An alternative interpretation in terms of pseudo-twins failed. Also the formation of the Ti_3Al phase and the corresponding $TiAl/Ti_3Al$ interfaces during the heat treatment or creep of the investigated alloy is not likely in view of the alloy composition.

TEM micrographs in Fig. 5 illustrate more complicated arrangements of deformation twins observed in later stages of creep. Figure 5a zooms an area where two systems of deformation twins that spread in different {111} planes cross each other. The deformation energy stored in the region of intersection facilitates the nucleation and growth of small fresh gamma grains. We note that these early stages of the recrystallization process were detected in the highly deformed regions like the one in Fig. 5a after creep strain higher than 5 %. Further growth of the recrystallized grains in twinned areas during creep resulted in partially recrystallized microstructure observed after 36 % of creep strain and documented in Fig. 5b. A

typical size of recrystallized grains was in the 1 μm range. Similar results were already reported for some near-gamma alloys with duplex microstructure crept in the temperature range between 923 and 1023 K [10, 11]. The clear conclusion supported by all these investigations is that a link exists between deformation twinning and the recrystallization process no matter whether we study creep in the pure gamma TiAl phase or in near-gamma TiAl based alloys.

4. Discussion

The most important reason for the co-operation of different deformation modes during creep in gamma TiAl phase is the need to fulfil the von Mises criterion [12]. The criterion requires five independent shear systems to be activated to preserve a compatibility of deformation. From this point of view, the orientation of the crystal lattice in different grains with respect to the axis of the applied compression stress favours different combinations of dislocation and twinning shears. As a result, various microstructures co-exist in the specimen during creep of the investigated compound.

The 3D dislocation network clearly results from a glide motion of ordinary dislocations and superdislocations. As it was already mentioned in the Section 3.1, several reasons can be suggested in order to understand the alignment of dislocations along certain crystallographic directions. The adopted procedure of the TEM dislocation contrast analysis does not allow a unique determination of dislocations in terms of their Burgers vectors. However, the observed dislocation contrast indicates a dissociation of some dislocation cores that can be characteristic for superdislocations. We note that the superdislocations were detected in a relevant amount also in the previous study where their densities represented an important fraction of the overall dislocation density, see Ref. [2].

The sub-boundaries result from a static or dynamic recovery that could take place during the HIP treatment and also during subsequent creep exposure. Those boundaries built exclusively by ordinary dislocations in the form of a square-shaped network, Fig. 2, are energetically neutral and thus no segment of a "nodal" dislocation reaction is formed. The sub-boundary separates regions rotated about the direction [001]. Undoubtedly this is not the only possible misorientation which could be observed in the gamma TiAl grains, also crystal lattice rotations about other axes should be accommodated by sub-boundaries. A single long sub-boundary in a field of the 3D network shown in Fig. 3 can serve as an example. The change of contrast across the boundary suggests that it separates misoriented regions. A waved character of sub-boundaries that do not follow any exact crystal plane was also observed in copper single crystals [13]. The full analysis of dislocations composing the boundary as well as the analysis of the corresponding structure in the neighbouring dense 3D dislocation network still represents a challenge. However,

the suggested dislocation reactions derived from our contrast analysis are neutral or energetically favourable and can thus be realistic.

In contrast to many metal and alloy systems investigated so far, deformation twinning plays very important role during creep in gamma TiAl intermetallics. This process is activated in appropriately oriented grains where it supplies the missing shear displacements required by the von Mises criterion. The task of the present work was to test the character of twins (to prove that they are not pseudo-twins or even lamellae of the Ti_3Al phase) and to present several examples of complex twinned structures. The fact that the twin boundaries can support the nucleation of new fresh gamma grains and thus facilitate recrystallization confirms a presence of internal stress fields in their vicinity.

5. Summary

Three microstructural types formed in parallel in the Ti-52Al intermetallic compound during creep at 1100 K under relatively high applied stress of 250 MPa. Although not fully representative, the analysis has shown that these microstructures result from the interplay of various shear systems, realized by the glide of ordinary dislocations and superdislocations as well as by the generation and growth of deformation twins. The demonstrated examples are probably not the only microstructural types that can exist. Different combinations of the shear systems activated during the compatible deformation in gamma TiAl may result in even wider spectrum of microstructures.

REFERENCES

[1] ČADEK, J.: Creep in Metallic Materials. Prague, Academia 1988, p. 95.
[2] ORLOVÁ, A.—KUCHAŘOVÁ, K.—DLOUHÝ, A.: Z. Metallkde, *95*, 2004, p. 1011.
[3] YAMAGUCHI, M.—UMAKOSHI, Y.: Prog. Mat. Sci., *34*, 1990, p. 1.
[4] DLOUHÝ, A.—EGGELER, G.: Pract. Metallography, *33*, 1996, p. 629.
[5] VÍTEK, V.: Intermetallics, *6*, 1998, p. 579.
[6] GRÉGORI, F.—VEYSSIÉRE, P.: Mat. Sci. Eng., *A309–331*, 2001, p. 87.
[7] GREENBERG, B. A.—ANISIMOV, V. I.—GORNOSTIREV, Y. N.—TALUTS, G. G.: Scripta Metal., *22*, 1988, p. 859.
[8] VISWANATHAN, G. B.—VASUDEVAN, V. K.—MILLS, M. J.: Acta Mater., *47*, 1999, p. 1399.
[9] KARTHIKEYAN, S.—VISWANATHAN, G. B.—GOUMA, P. I.—VASUDEVAN, V. K.—KIM, Y.-W.—MILLS, M. J.: Mat. Sci. Eng., *A329–331*, 2002, p. 621.
[10] SKROTZKI, B.—ÜNAL, M.—EGGELER, G.: Scripta Mater., *39*, 1998, p. 1023.

[11] SKROTZKI, B.—RUDOLF, T.—DLOUHÝ, A.—EGGELER, G.: Scripta Mater., *39*, 1998, p. 1545.
[12] v. MISES, R.: Zeit. Ang. Math. u. Mech., *8*, 1928, p. 161.
[13] ORLOVÁ, A.: Z. Metallkde, *92*, 2001, p. 76.